Supporting Information

Solid-Phase Hot-Pressing Synthesis of POMOFs on Carbon Cloth and Derived Phosphides for All pH Values Hydrogen Evolution

Yu-Jia Tang,[a]‡ Yifa Chen,[a]‡ Hong-Jing Zhu,[a] A-Man Zhang,[a] Xiao-Li Wang,[a] Long-Zhang Dong,[a] Shun-Li Li,[a] Qiang Xu,*[b] and Ya-Qian Lan*[a]

[a]Jiangsu Collaborative Innovation Centre of Biomedical Functional Materials, Jiangsu Key Laboratory of New Power Batteries, School of Chemistry and Materials Science, Nanjing Normal University, Nanjing 210023, China.

[b]Research Institute of Electrochemical Energy, National Institute of Advanced Industrial Science and Technology (AIST), Ikeda, Osaka 563-8577, Japan

Corresponding Author

yqlan@njnu.edu.cn; q.xu@aist.go.jp

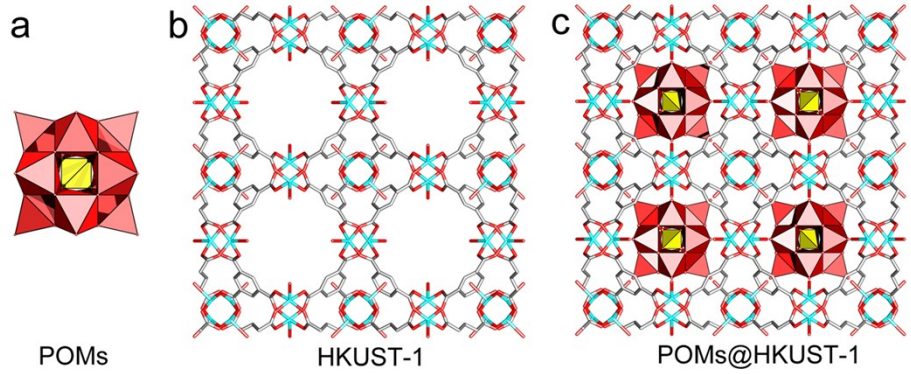

Figure S1. The crystal structure of (a) POMs, (b) HKUST-1 and (c) POMs@HKUST-1.

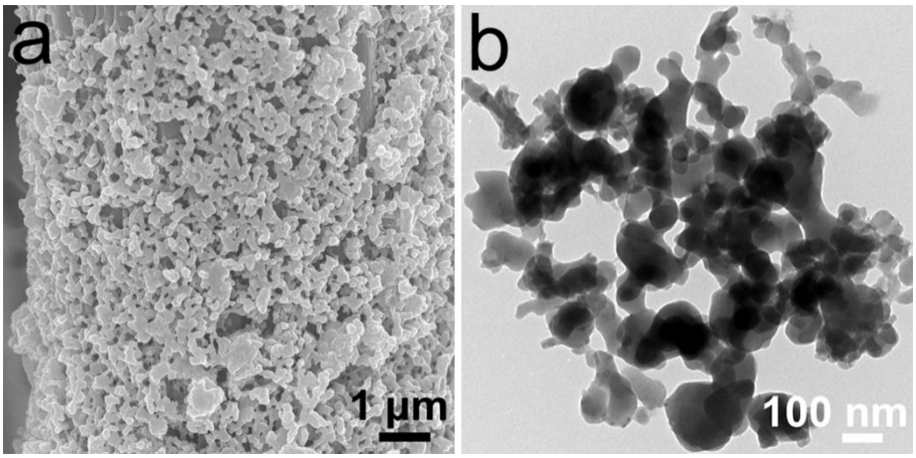

Figure S2. (a) SEM image of PMo_{12}@HKUST-1/CC, (b) TEM image of PMo_{12}@HKUST-1 sonicated from CC.

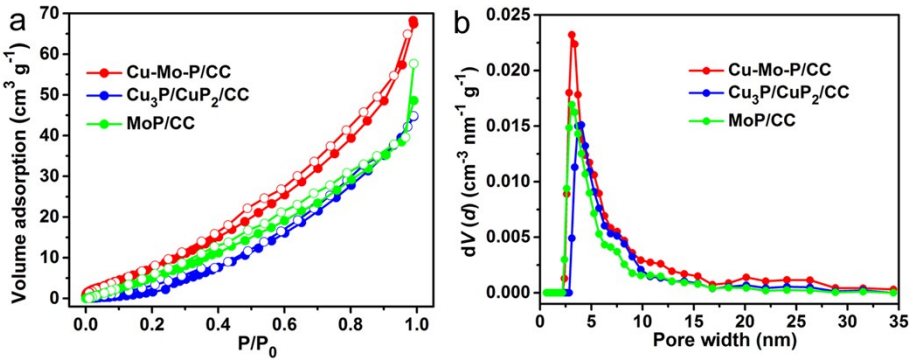

Figure S3. (a) Nitrogen adsorption-desorption isotherms of Cu-Mo-P/CC, Cu_3P/CuP_2/CC and MoP/CC conducted at 77 K. (b) Pore size distributions of Cu-Mo-P/CC, Cu_3P/CuP_2/CC and MoP/CC fitted to the model of nitrogen at 77 K on carbon (slit pore, QSDFT equilibrium model) with the small fitting error(< 7%).

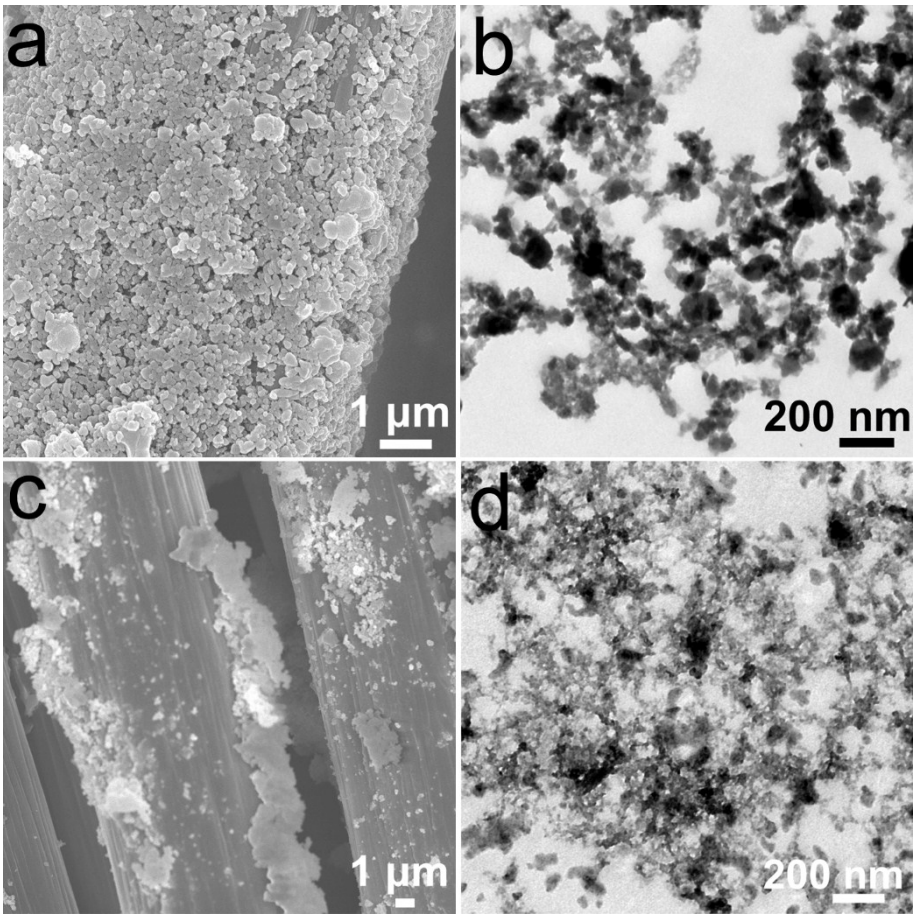

Figure S4. (a) SEM image of HKUST-1/CC, (b) TEM image of HKUST-1 sonicated from CC. (c) SEM image of PMo_{12}/CC, (d) TEM image of PMo_{12} sonicated from CC.

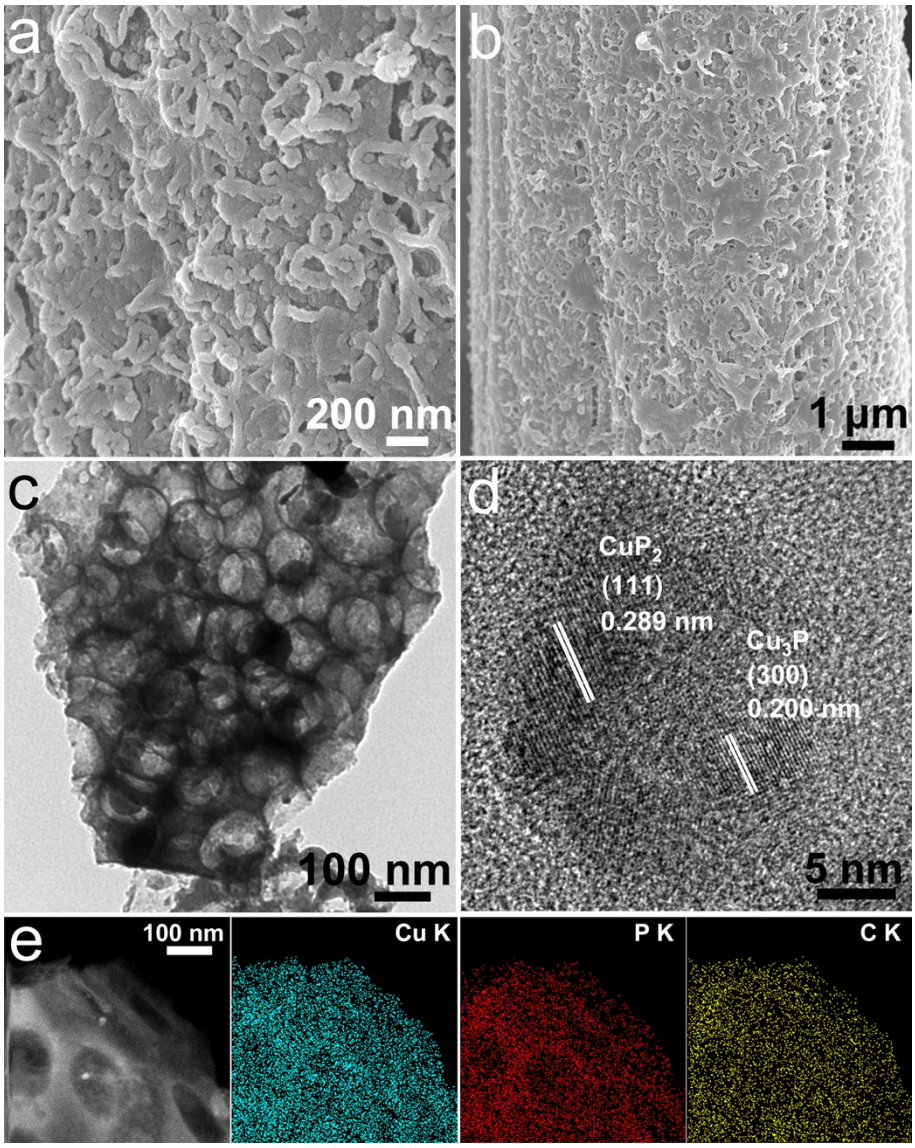

Figure S5. (a), (b) SEM images of $Cu_3P/CuP_2/CC$. (c) TEM and (d) HRTEM images of Cu_3P/CuP_2 sonicated from CC. The lattice spacings of 0.200 nm and 0.289 nm are assigned to the (300) plane of Cu_3P and (111) plane of CuP_2, respectively. (e) HAADF image and corresponding element mappings, Cu, P and C are shown in blue, red and yellow, respectively.

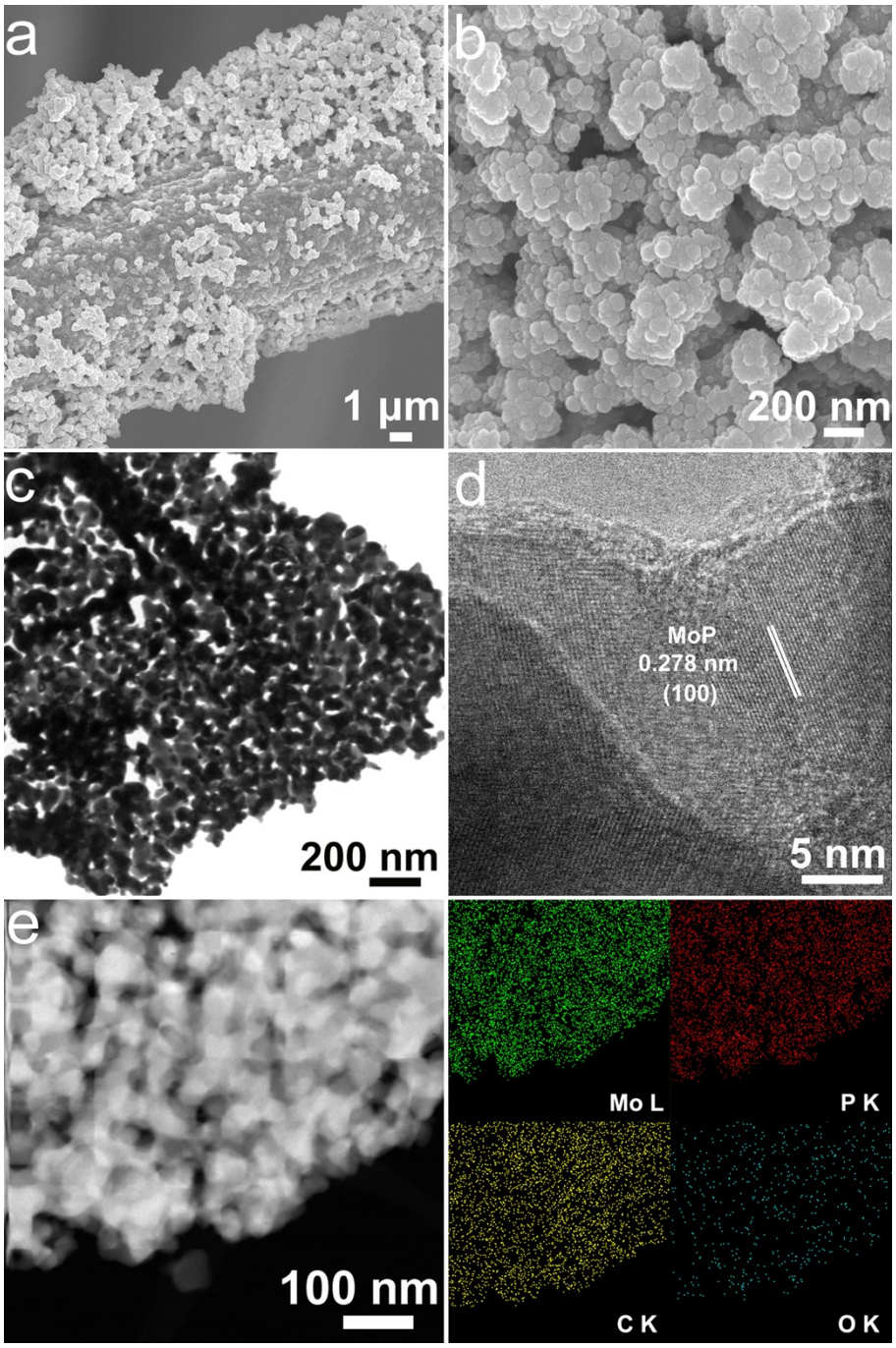

Figure S6. (a), (b) SEM images of MoP/CC. (c) TEM and (d) HRTEM image of MoP sonicated form CC. The lattice spacing of 0.278 nm is assigned to the (100) plane of MoP. (e) HAADF image and corresponding element mappings, Mo, P and C are shown in green, red and yellow, respectively.

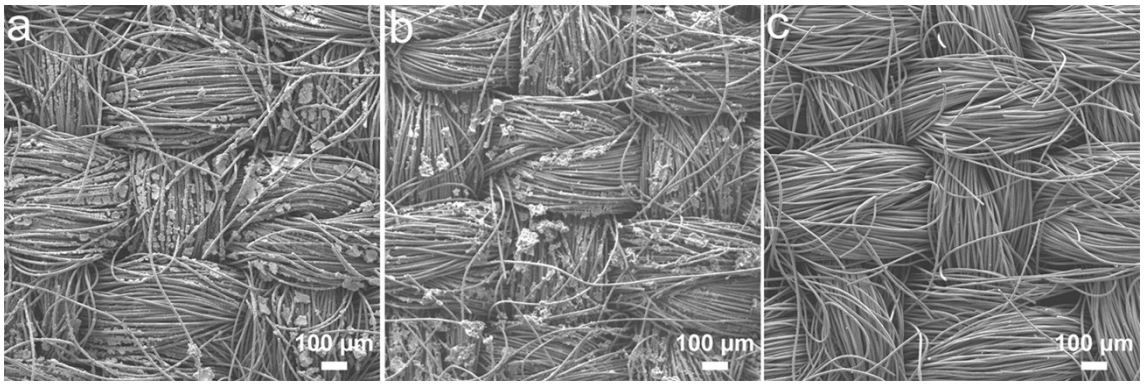

Figure S7. SEM images of (a) Cu-Mo-P/CC, (b) Cu_3P/CuP_2/CC and (c) MoP/CC in the large scale.

Cu-Mo-P/CC and Cu_3P/CuP_2/CC show some agglomerates on the surface of CC in the large scale. After phosphidation, the POMOFs precursors floated on CC can turn into the Cu-Mo-P agglomerates due to the existence of carbon sources mainly derived from the BTC ligands. According to the SEM image in Figure 3b and Figure S5, every carbon fiber for Cu-Mo-P/CC shows the densely and uniformly decorated Cu-Mo-P particles. These agglomerates should be the excess Cu-Mo-P phosphides on CC, which can't coat on every carbon fiber anymore. Therefore, the large area SEM image of Cu-Mo-P/CC proves the advantages of the solid-phase hot-pressing method for the growth of Cu-Mo-P without stacking. In contrast, SEM image of MoP/CC exhibits no agglomerates on CC because of only little carbon source from PEG.

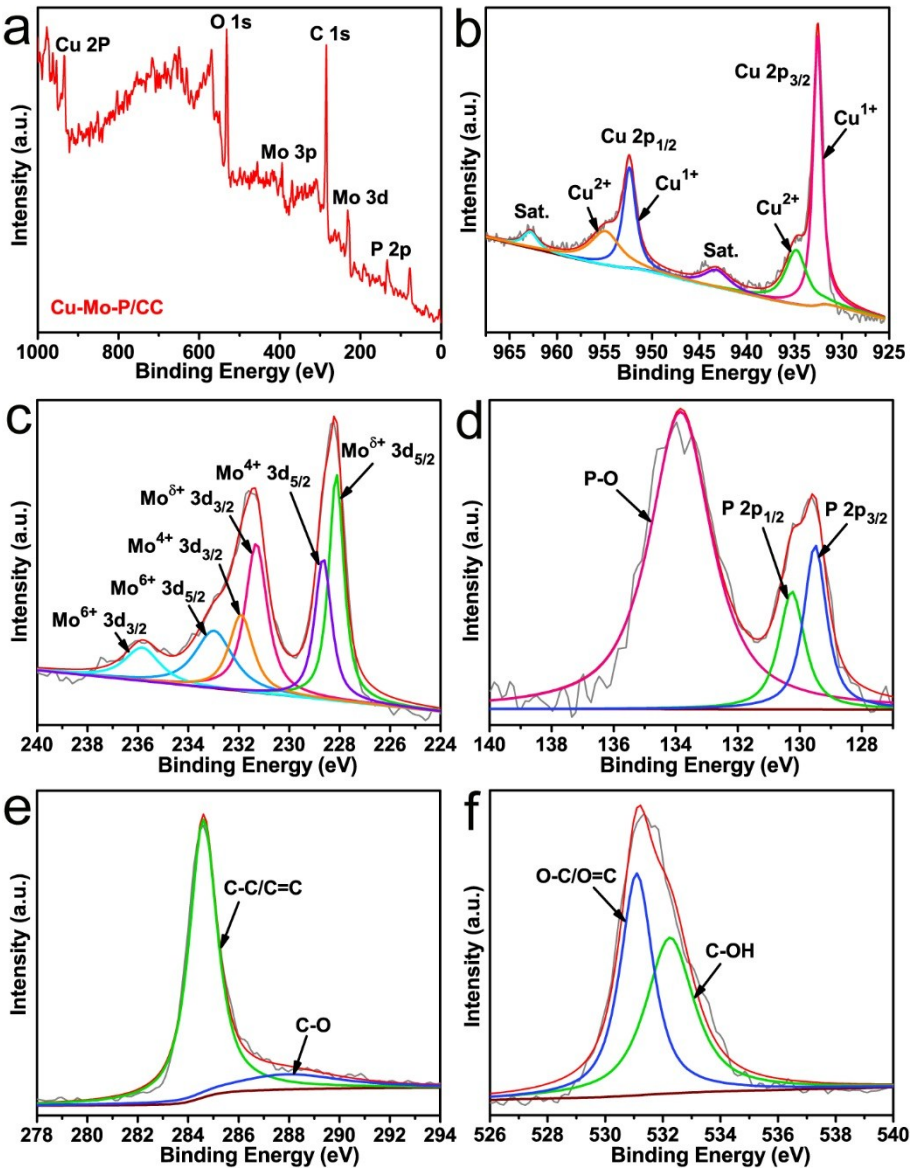

Figure S8. XPS spectrum of (a) Cu-Mo-P/CC. High resolution XPS spectra of (b) Cu 2p, (c) Mo 3d, (d) P 2p, (e) C 1s and (f) O 1s.

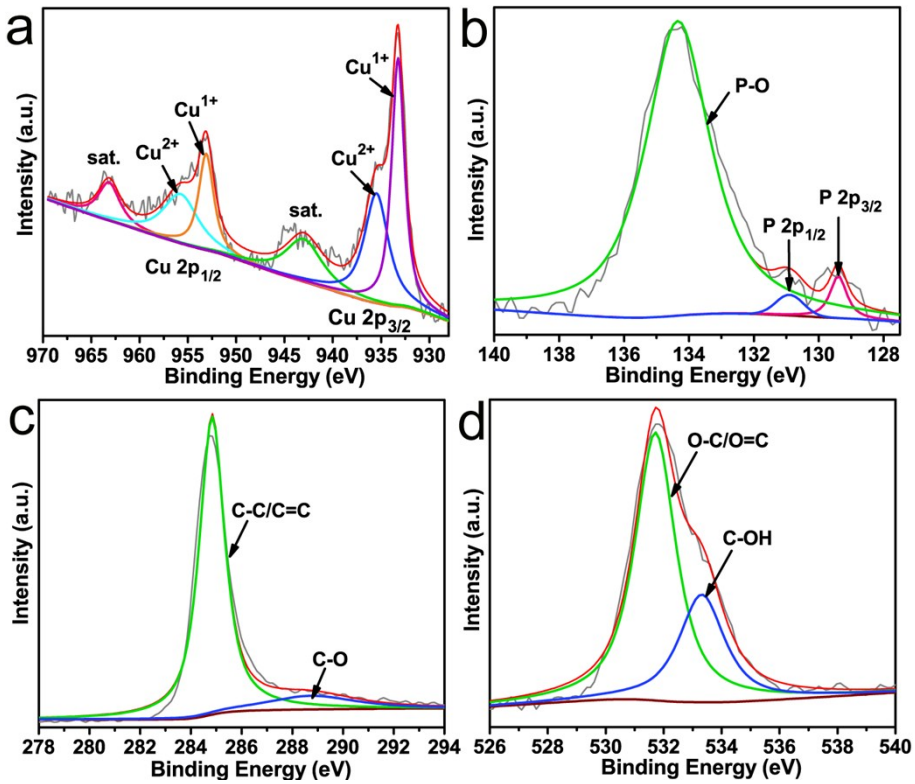

Figure S9. High resolution XPS spectra of (a) Cu 2p, (b) P 2p, (c) C 1s and (d) O 1s for $Cu_3P/CuP_2/CC$.

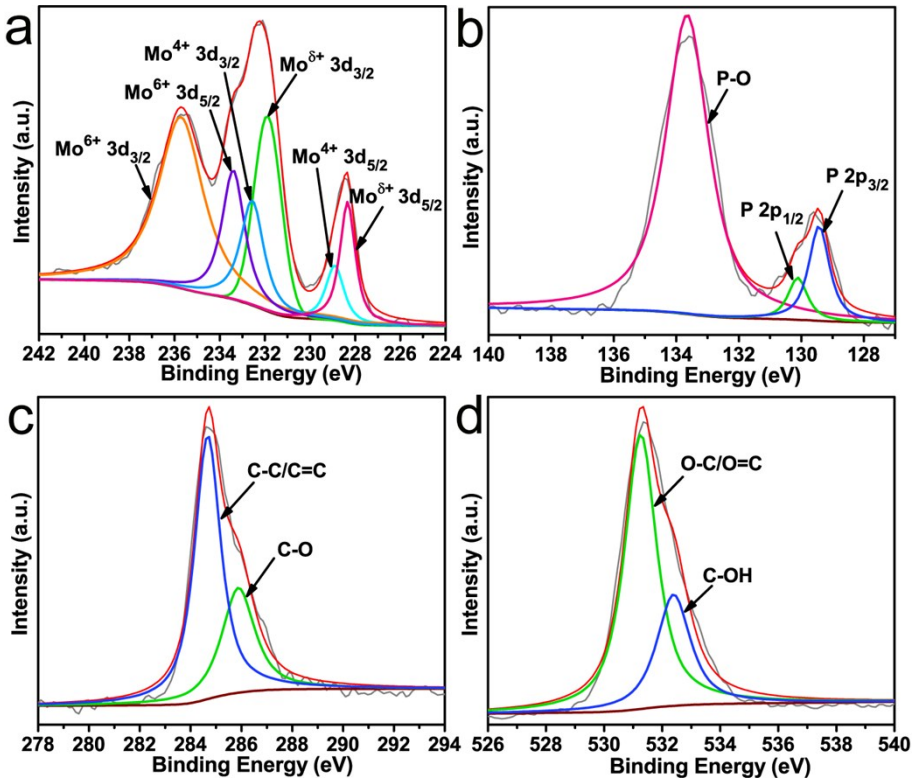

Figure S10. High resolution XPS spectra of (a) Mo 3d, (b) P 2p, (c) C 1s and (d) O 1s for MoP/CC.

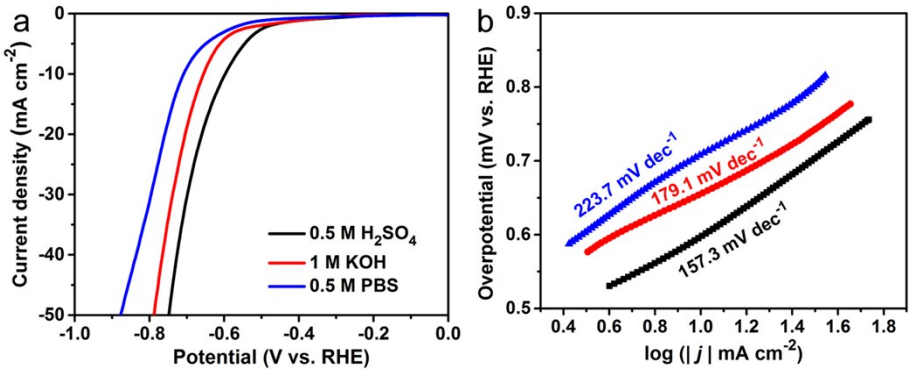

Figure S11. (a) LSV curves of bare CC tested at different electrolytes, (b) corresponding Tafel slopes.

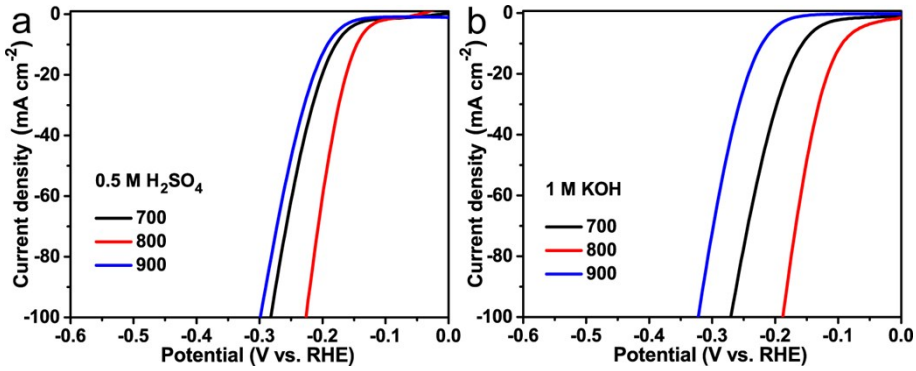

Figure S12. LSV curves of Cu-Mo-P/CC synthesized at different phosphidation temperatures (700, 800 and 900 °C) in (a) 0.5 M H_2SO_4 and (b) 1 M KOH.

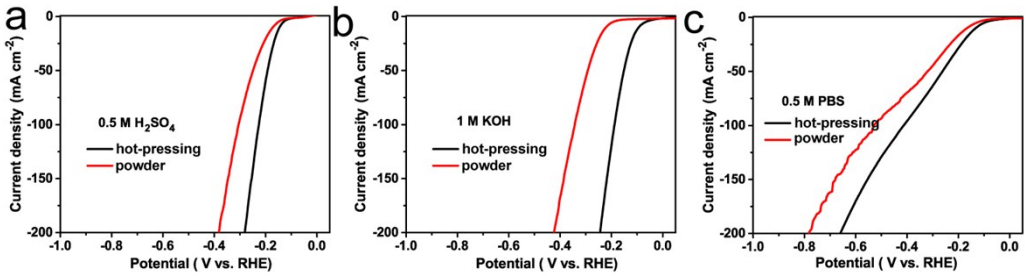

Figure S13. LSV curves of Cu-Mo-P/CC prepared using hot-pressing method and Cu-Mo-P powder prepared using solution method in (a) 0.5 M H_2SO_4, (b) 1 M KOH and (c) 0.5 M PBS.

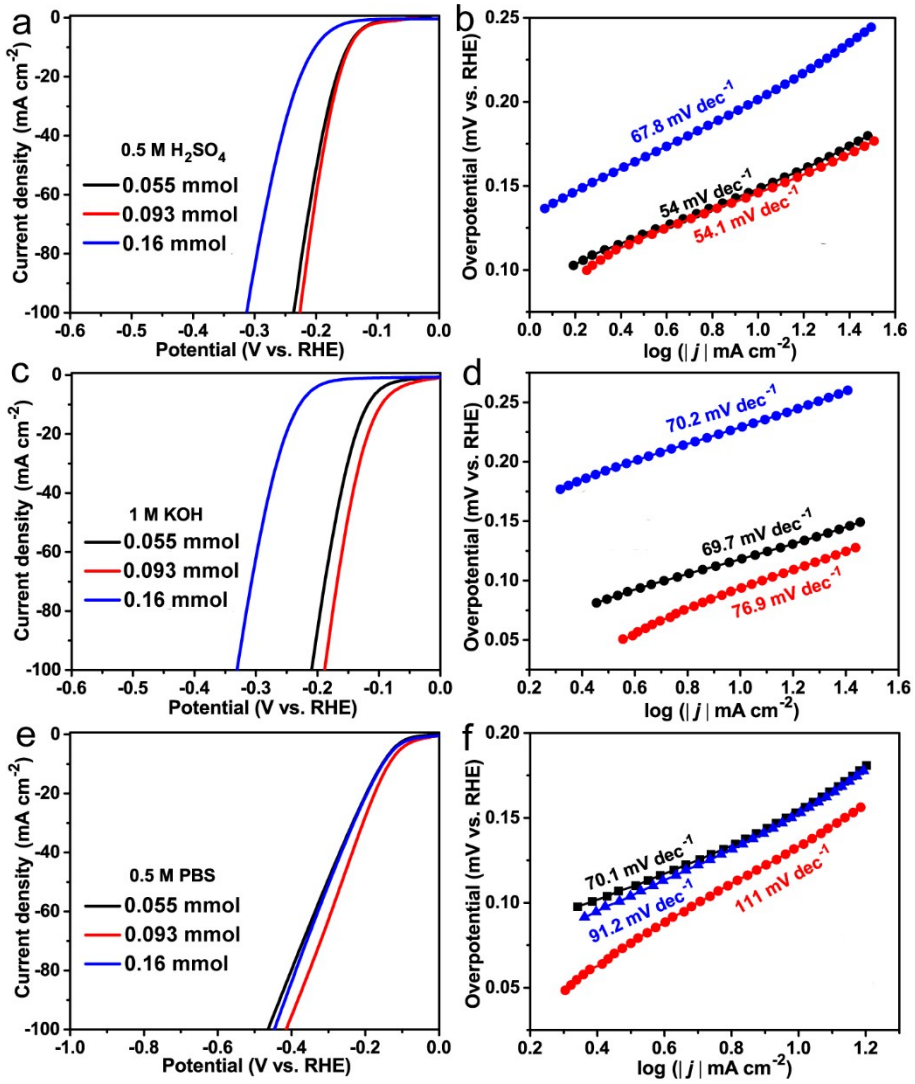

Figure S14. LSV curves and Tafel plots of Cu-Mo-P/CC prepared using different PMo_{12} loadings in (a) and (b) 0.5 M H_2SO_4, (c) and (d) 1 M KOH, (e) and (f) 0.5 M PBS.

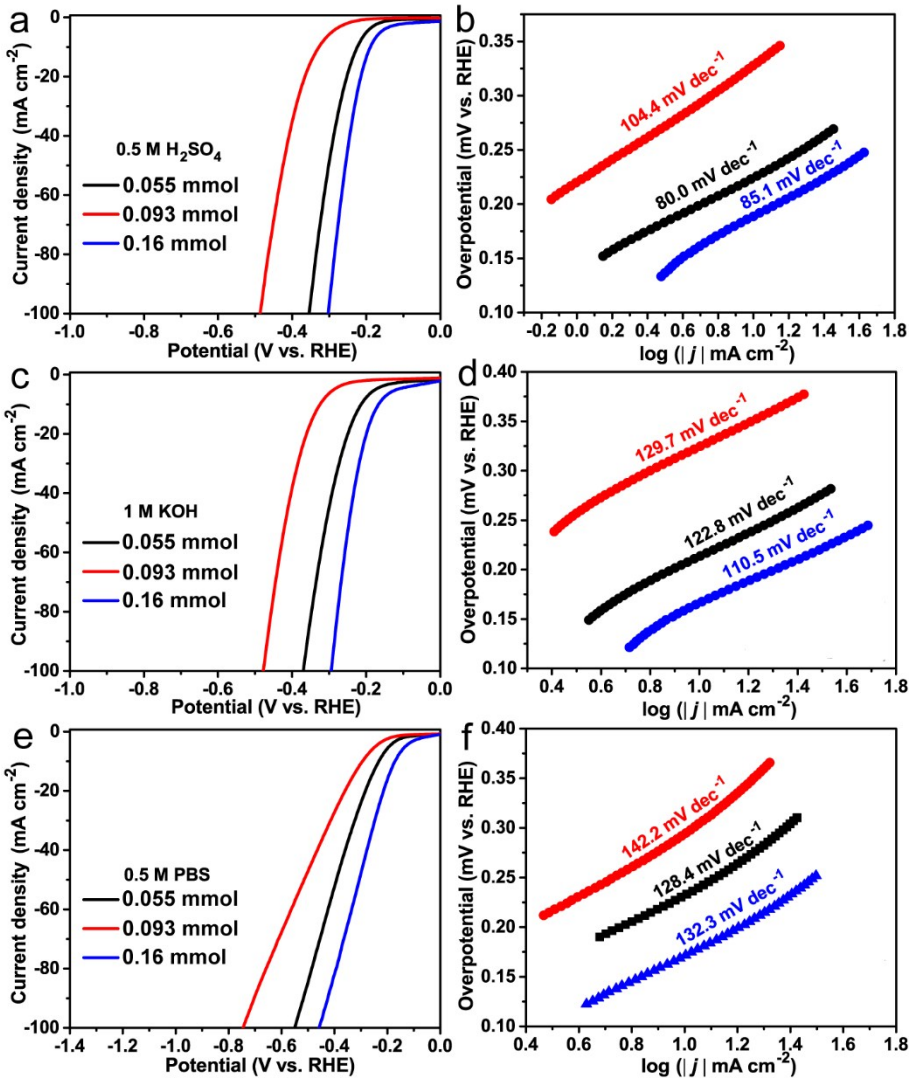

Figure S15. LSV curves and Tafel plots of Cu-W-P/CC prepared using different PW_{12} loadings in (a) and (b) 0.5 M H_2SO_4, (c) and (d) 1 M KOH, (e) and (f) 0.5 M PBS.

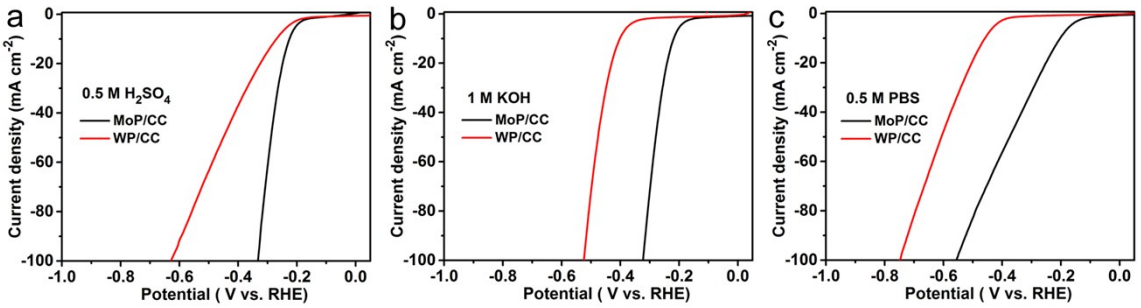

Figure S16. LSV curves of MoP/CC and WP/CC prepared using POMs loadings of 0.092 mmol in (a) 0.5 M H_2SO_4, (b) 1 M KOH, (c) 0.5 M PBS.

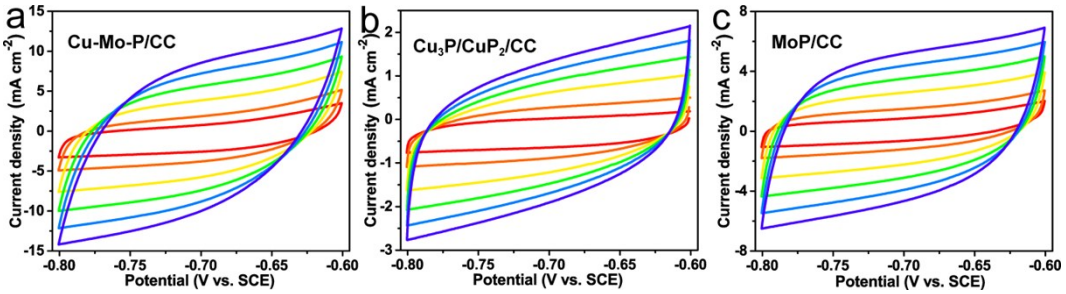

Figure S17. CV curves between the potential of -0.8 and -0.6 V vs. SCE at different scan rate (10-100 mV s^{-1}) in 1 M KOH for (a) Cu-Mo-P/CC, (b) Cu_3P/CuP_2/CC and (c) MoP/CC.

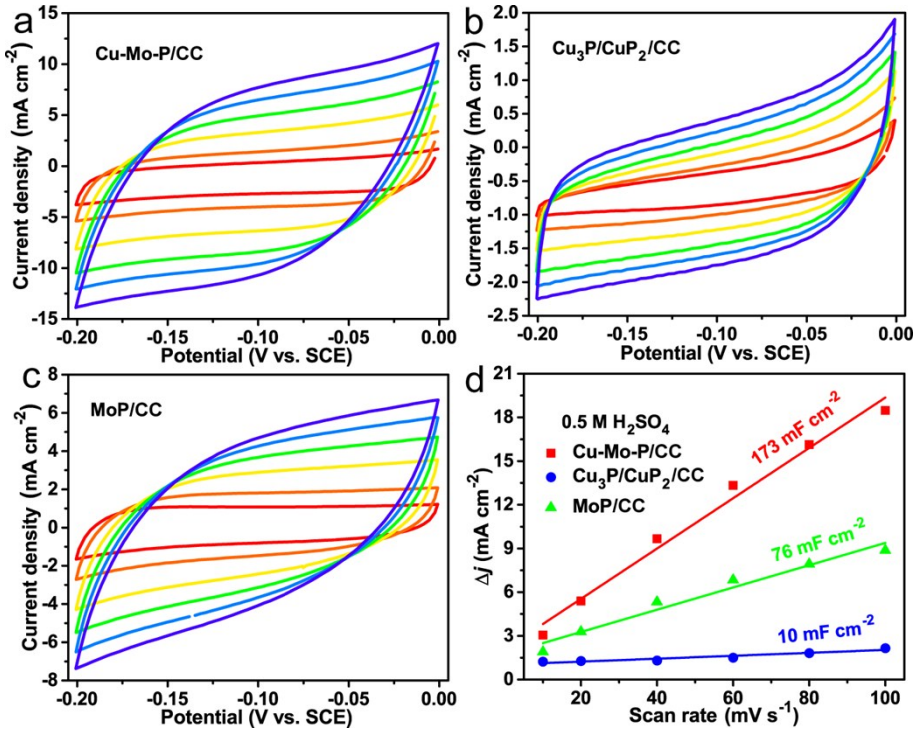

Figure S18. CV curves between the potential of -0.2 and 0 V vs. SCE at different scan rate (10-100 mV s^{-1}) in 0.5 M H_2SO_4 for (a) Cu-Mo-P/CC, (b) Cu_3P/CuP_2/CC and (c) MoP/CC. (d) C_{dl} calculated according to the CV curves.

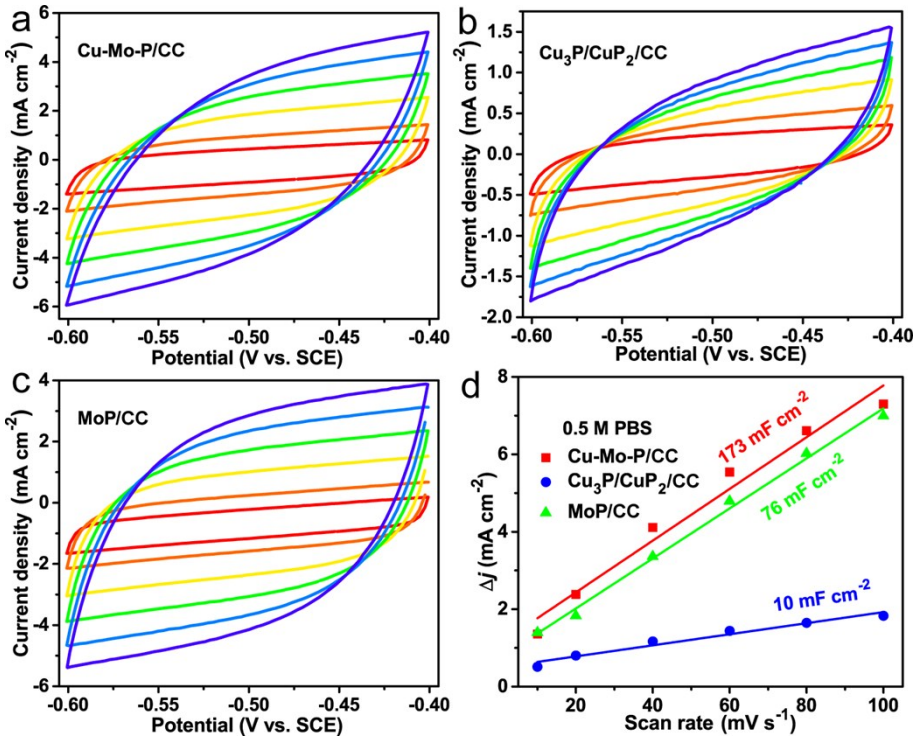

Figure S19. CV curves between the potential of -0.6 and -0.4 V vs. SCE at different scan rate (10-100 mV s^{-1}) in 0.5 M PBS for (a) Cu-Mo-P/CC, (b) Cu_3P/CuP_2/CC and (c) MoP/CC. (d) C_{dl} calculated according to the CV curves.

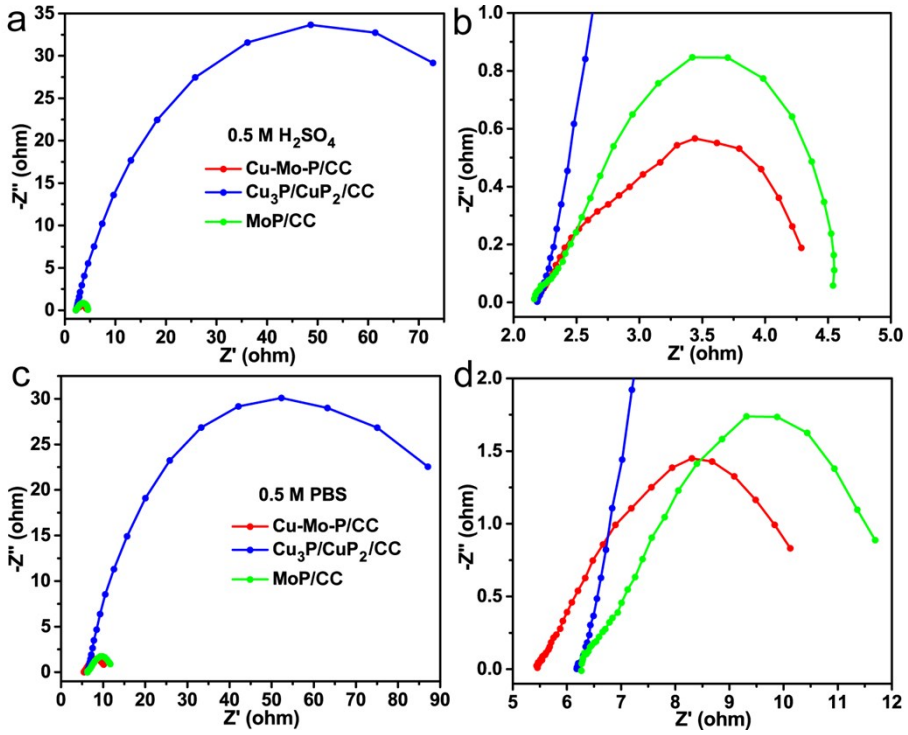

Figure S20. EIS spectra of Cu-Mo-P/CC, Cu_3P/CuP_2/CC and MoP/CC recorded at the overpotential of 150 mV vs. RHE for HER (a) in 0.5 M H_2SO_4, (b) the enlarged spectrum of (a), (c) in 0.5 M PBS, (d) the enlarged spectrum of (c).

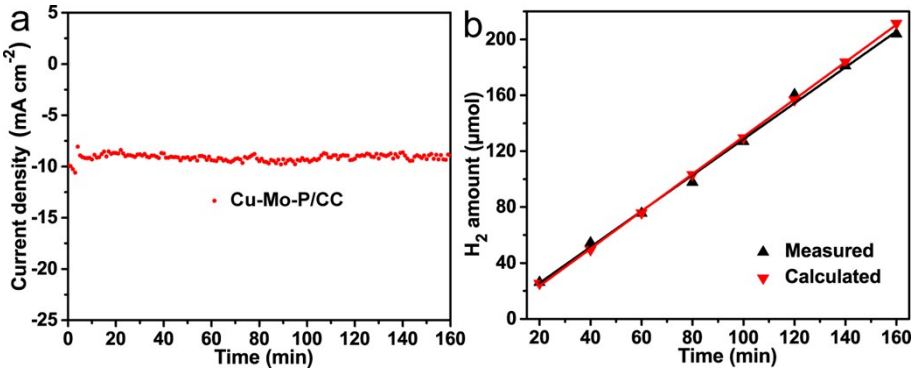

Figure S21. (a) Chronoamperometric curve of Cu-Mo-P/CC at fixed potential to reach the current density of 10 mA cm^{-2} in 1 M KOH for FE test. (b) The amounts of H_2 measured theoretically and experimentally.

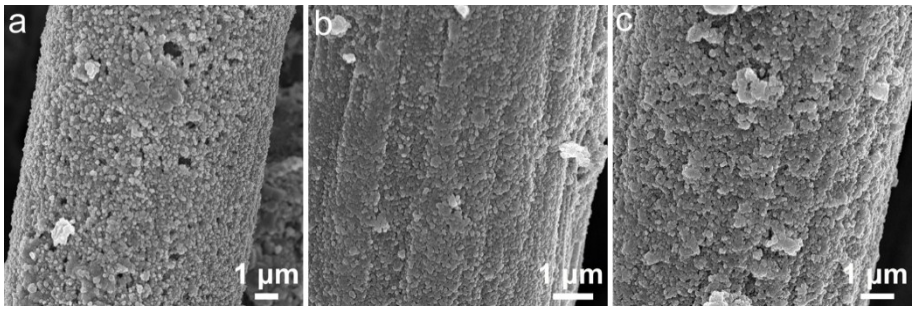

Figure S22. SEM images of Cu-Mo-P/CC after CA stability test for 20 h in (a) 0.5 M H_2SO_4, (b) 1 M KOH and (c) 0.5 M PBS.

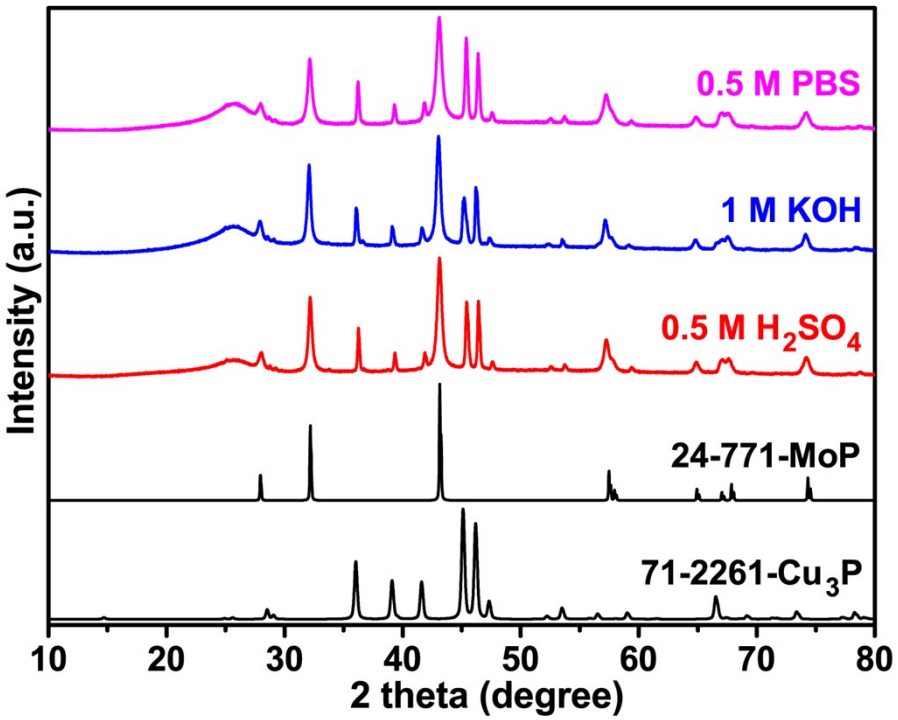

Figure S23. PXRD pattern of Cu-Mo-P/CC composite after CA stability test in different electrolytes. PXRD patterns Cu-Mo-P/CC after test in three electrolytes all show the disappearance of CuP_2 but reservation of primary Cu_3P and MoP, indicating the instability of CuP_2 during the electrocatalytic reaction.

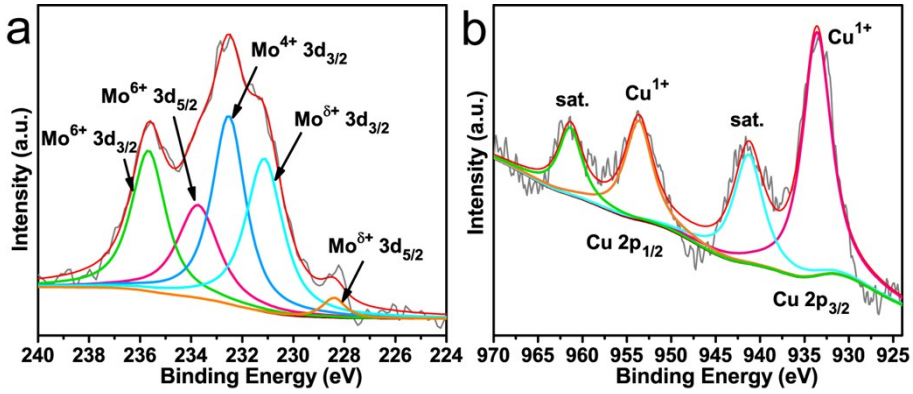

Figure 24. XPS spectra of Cu-Mo-P/CC composite after CA stability test in 0.5 M H_2SO_4 for (a) Mo 3d spectrum and (b) Cu 2p spectrum. Mo 3d spectrum of Cu-Mo-P after CA test in acid solution can be deconvoluted into five peaks assigning to MoP and molybdenum oxides. However, Cu^{2+} peaks are disappeared in Cu 2p spectrum, indicating the conversion of CuP_2 into Cu_3P.

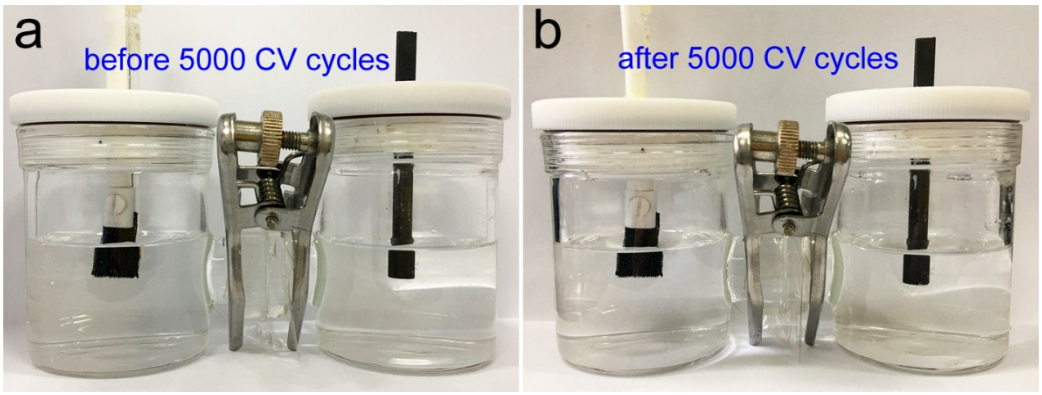

Figure S25. Photographs of Cu-Mo-P/CC in 0.5 M H_2SO_4 (a) before and (b) after 5000 CV cycles test.

Table S1. The tatol mass of bare CC and Cu-Mo-P/CC and the averge mass loading of Cu-Mo-P catalyst (the area of CC is 1 × 2 cm^{-2}).

	1	2	3	4
Bare CC (mg)	2.61	2.63	2.53	2.60
Cu-Mo-P/CC (mg)	5.29	5.45	5.19	5.40
Cu-Mo-P catalyst (mg)	2.68	2.82	2.66	2.80
Average mass loading (mg cm^{-2})			1.37	

Table S2. Atomic percent (%) of corresponding samples by XPS analysis.

	Cu 2p	Mo 3d	P 2p	C 1s	O 1s
Cu-Mo-P/CC	2.24	2.86	8.01	66.85	20.04
$Cu_3P/CuP_2/C$ C	2.07	/	4.95	79.65	13.33
MoP/CC	/	10.45	11.88	31.95	45.72

Table S3. Comparison of η_{10} and Tafel Slope of corresponding samples in the manuscript for all pH values HER performance.

Samples	HER parameter	0.5 M H_2SO_4	1 M KOH	0.5 M PBS
Cu-Mo-P/CC	η_{10} (mV vs. RHE)	145.9	**90.5**	132.6
	Tafel slope (mV dec^{-1})	**54.1**	76.9	111
$Cu_3P/CuP_2/CC$	η_{10} (mV vs. RHE)	266.1	358.7	294.8
	Tafel slope (mV dec^{-1})	86.9	162.1	105
MoP/CC	η_{10} (mV vs. RHE)	223.6	220.2	202.2
	Tafel slope (mV dec^{-1})	74.2	72.2	109
Cu-W-P/CC (0.16 mmol PW_{12})	η_{10} (mV vs. RHE)	187.4	163.9	172.0
	Tafel slope (mV dec^{-1})	85.1	110.5	132.3

Table S4. Comparison of HER performance of Cu-Mo-P/CC and recently reported MOFs-derived materials and other phosphides on conductive substrates as HER electrocatalysts at different electrolytes.

Electrocatalyst	Substrate	Electrolyte	η_{10} (mV vs. RHE)	Tafel slope (mV dec^{-1})	Reference
Cu-Mo-P/CC	Carbon cloth	0.5 M H_2SO_4	145.4	**54.1**	This work
		1 M KOH	**90.5**	76.9	
		0.5 M PBS	132.6	111	
Ni-Fe-P@C	Ni foam	1 M KOH	79	92.6	[1]
Co-Ni-Se/C/NF	Ni foam	1 M KOH	90	81	[2]
$CoSe_2$/CF	Carbon fiber paper	1 M KOH	95	52	[3]
ZIF@LDH@Ni foam-600	Ni foam	1 M KOH	106	109	[4]
Ni@CoO@CoNC	Ni foam	1 M KOH	190	98	[5]
CoS_2 NTA/CC	Carbon cloth	1 M KOH	193	88	[6]
Co@NC	Ni foam	0.1 M KOH	240	126.8	[7]
Cu_3P NW/CF	Copper foam	0.5 M H_2SO_4	143	67	[8]
WP NAs/CC	Carbon cloth	0.5 M H_2SO_4	130	69	[9]
		1 M KOH	150	102	
		1 M PBS	200	125	
CoP/CC	Carbon cloth	0.5 M H_2SO_4	67	51	[10]
		1 M KOH	209	129	
		1 M PBS	106	93	
CuCo@NC	Glass carbon electrode	0.5 M H_2SO_4	145	79	[11]
NiCoP@Cu_3P/CF	Cu foam	1 M KOH	54	72	[12]
Cu@NC NT/CF-500	Cu foam	1 M KOH	123	63	[13]
Cu_3P NB	Cu mesh	0.5 M H_2SO_4	120	72	[14]
		1 M KOH	252	150	

Table S5. R_{ct} values (Ω) recorded at the overpotential of 150 mV vs. RHE in different electrolytes.

	0.5 M H_2SO_4	1 M KOH	0.5 M PBS
Cu-Mo-P/CC	1.6	**0.96**	4
Cu_3P/CuP_2/CC	82.2	48.8	83.6
MoP/CC	1.8	1.3	5.8

Reference

1. S. H. Ahn and A. Manthiram, *J. Mater. Chem. A*, 2017, **5**, 2496-2503.
2. F. Ming, H. Liang, H. Shi, X. Xu, G. Mei and Z. Wang, *J. Mater. Chem. A*, 2016, **4**, 15148-15155.
3. C. Sun, Q. Dong, J. Yang, Z. Dai, J. Lin, P. Chen, W. Huang and X. Dong, *Nano Res.*, 2016, **9**, 2234-2243.
4. Y. Tang, X. Fang, X. Zhang, G. Fernandes, Y. Yan, D. Yan, X. Xiang and J. He, *ACS Appl. Mater. Interfaces*, 2017, **9**, 36762-36771.
5. G. Cai, W. Zhang, L. Jiao, S.-H. Yu and H.-L. Jiang, *Chem*, **2**, 791-802.
6. C. Guan, X. Liu, A. M. Elshahawy, H. Zhang, H. Wu, S. J. Pennycook and J. Wang, *Nanoscale Horiz.*, 2017, **2**, 342-348.
7. A. Aijaz, J. Masa, C. Rösler, W. Xia, P. Weide, R. A. Fischer, W. Schuhmann and M. Muhler, *ChemElectroChem*, 2017, **4**, 188-193.
8. J. Tian, Q. Liu, N. Cheng, A. M. Asiri and X. Sun, *Angew. Chem. Int. Ed.*, 2014, **53**, 9577-9581.
9. Z. Pu, Q. Liu, A. M. Asiri and X. Sun, *ACS Appl. Mater. Interfaces*, 2014, **6**, 21874-21879.
10. J. Tian, Q. Liu, A. M. Asiri and X. Sun, *J. Am. Chem. Soc.*, 2014, **136**, 7587-7590.
11. M. Kuang, Q. Wang, P. Han and G. Zheng, *Adv. Energy Mater.*, 2017, **7**, 1700193.
12. X. Ma, Y. Chang, Z. Zhang and J. Tang, *J. Mater. Chem. A*, 2018, **6**, 2100-2106.
13. Y. Zhang, Y. Ma, Y.-Y. Chen, L. Zhao, L.-B. Huang, H. Luo, W.-J. Jiang, X. Zhang, S. Niu, D. Gao, J. Bi, G. Fan and J.-S. Hu, *ACS Appl. Mater. Interfaces*, 2017, **9**, 36857-36864.
14. S. Wei, K. Qi, Z. Jin, J. Cao, W. Zheng, H. Chen and X. Cui, *ACS Omega*, 2016, **1**, 1367-1373.